International Journal of MATERIALS RESEARCH

Zeitschrift für METALLKUNDE

12/2009

100 ANNIVERSARY

Proceedings of the Workshop on New Advances in SPD Processing and Properties of Ductile Nanostructured Materials, June 1–4, 2009, Melbourne, Australia

Volume 100, Dezember 2009 www.ijmr.de HANSER

Cover photograph:
W. Xu, X. Wu., R. B. Figueiredo, M. Stoica, M. Calin, J. Eckert, T. G. Langdon, K. Xia
p. 1663

Editor

Deutsche Gesellschaft
für Materialkunde e. V.

DGM

Co-Editor

Société Française de
Métallurgie et de Matériaux

SF2M

Managing Editors

M. Rühle
G. Petzow
Max-Planck-Institut für Metallforschung, Heisenbergstr. 3
D-70569 Stuttgart, Germany

F. O. R. Fischer
DGM e. V., Senckenberganlage 10
D-60325 Frankfurt, Germany

Editorial Office

Viola Küstner
R. W. M. Segar
Max-Planck-Institut für Metallforschung
Heisenbergstr. 3
D-70569 Stuttgart, Germany
Tel.: +49 711 689 3651
Fax: +49 711 689 3653
E-mail: ijmr@mf.mpg.de

All correspondence concerning papers under review or already in production should be addressed to the **Editorial Office**.

Guest Editors

Kenong Xia, University Melbourne
Terence G. Langdon,
University of Southern California,
University of Southampton

HANSER

Carl Hanser Verlag GmbH & Co. KG
D-81631 Munich, Germany
http://www.hanser.de
E-mail: info@hanser.de
Distribution: +49 89 99 8 30-1 02
Advertising: +49 89 99 8 30-2 15

CONTENTS

Ilchat Sabirov[a], Matthew R. Barnett[b,c], Yuri Estrin[c,d], Ilana Timokhina[b], Peter D. Hodgson[b,c]

[a] Instituto Madrileño de Estudios Avanzados de Materiales (IMDEA-Materiales), E.T.S. de Ingenieros de Caminos, Madrid, Spain
[b] Centre for Material and Fibre Innovation, Deakin University, Waurn Ponds, Victoria, Australia
[c] ARC Centre of Excellence for Design in Light Metals, Department of Materials Engineering, Monash University, Clayton, Victoria, Australia
[d] CSIRO Division of Process Science and Engineering, Clayton South, Victoria, Australia

Deformation mechanisms in an ultra-fine grained Al alloy

This work focuses on the deformation behavior of an ultra-fine grained Al–Mg–Si alloy processed by equal channel angular pressing over a wide range of temperatures and strain rates. The effect of temperature and strain rate on the homogeneity of plastic deformation, the evolution of microstructure, the strain rate sensitivity and the underlying deformation mechanisms are investigated. It is demonstrated that the localization of plastic deformation at the micro scale is triggered by grain boundary sliding due to grain boundary diffusion. The contributions of different deformation mechanisms during the plastic deformation of the material are discussed.

Keywords: Al alloy; Equal channel angular pressing; Ultra-fine grained microstructure; Deformation mechanisms

1. Introduction

The refinement of the microstructure of metallic materials down to the ultra-fine and nanoscale by severe plastic deformation (SPD) is now a well-established approach to processing [1]. Equal-channel angular pressing (ECAP) is the most widely used SPD method [2]. Grain refinement during ECAP is believed to be associated with the formation of dislocation cells, which then evolve to subgrains and grains. ECAP processing of Al alloys is of special interest due to their light weight. They also possess a favorable combination of mechanical properties [3]. However, the use of Al alloys has been limited by their strength not being sufficient for high-end applications. The strength of Al alloys can be greatly enhanced via SPD processing, but at the cost of degraded ductility [4]. The tensile ductility of ultra-fine grained (UFG) and nanocrystalline metals and alloys can be improved by various strategies [5]. The activation of certain deformation mechanisms along with suppression of others through microstructural design or by manipulating deformation parameters can significantly increase the uniform elongation. One example is the development of bimodal microstructures, where coarse grains (with a size of a few microns) are embedded in a matrix with ultrafine or nanosized grains. Bimodality can significantly increase the uniform elongation [6, 7], supposedly due to the localization of plastic deformation in the coarser grains, which delays the onset of necking. An example of a bimodal grain structure giving rise to a combination of high yield strength and reasonably good ductility is alloy Al5083 processed through mixing of cryomilled nanostructured powder with unmilled coarse-grained powder, followed by consolidation through extrusion [8].

Another approach to improve the ductility of UFG and nanostructured metals is based on the idea of testing them at higher strain rates and/or lower temperatures [7]. Plastic deformation at low (cryogenic) temperatures results in an increased work hardening rate due to reduced dislocation annihilation both at grain boundaries and in the bulk (by thermally activated cross slip and climb) [7]. This delays the onset of necking, thus increasing tensile uniform elongation. Testing at high strain rates has a similar effect in terms of promoting strain hardening. The third strategy is to introduce tiny second-phase particles into ultra-fine or nano-grains [9, 10]. Introduction of second phase nano-precipitates (η'- and η-phases) with a size of about 10 nm in ultra-fine grains with an average size of 100 nm in an Al7075 alloy resulted in an increase of the uniform elongation from 3.3 % to 7.4 % – with a simultaneous increase of the yield strength from 550 to 615 MPa [9]. Nano-precipitates provided additional strengthening by the Orowan mechanism and increased strain hardening. A similar effect was observed in an ultra-fine-structured Al2119 alloy subjected to cryo-rolling and low temperature annealing [10]. A further strategy is based on utilization of elevated strain rate sensitivity. According to the well known Hart criterion [11], increased strain rate sensitivity offers more resistance to localization of plastic deformation at the macro scale.

The present work focuses on the increased ductility seen when the processing conditions are optimized. The work analyses the deformation behavior of an ECAP processed ultra-fine grained Al–Mg–Si alloy over a wide range of temperatures and strain rates. The deformation mechanisms operating during plastic deformation and the strain rate sensitivity are examined.

2. Experimental procedures

Commercial grade Al–Mg–Si alloy (AA6082) of composition (in wt.%) 1 Mg, 1 Si, 0.4 Cu and balance Al was used for this investigation. Rods with the dimensions of

100 mm × 10 mm × 10 mm were solution treated at 530 °C for 2 h and quenched in water. Each sample was subjected to eight ECAP passes at 100 °C using route B_c (with a rotation of 90° about the pressing direction after each pass in a die with an internal channel angle $\varphi = 90°$ and outer angle $\psi = 0°$ [2]). The strain produced in each pass was about 1, so that the cumulative strain the specimen underwent as a result of the ECAP processing was about 8. After ECAP processing, the specimens were kept for one week at ambient temperature (naturally aged).

To study the microstructure, transmission electron microscopy (TEM) was carried out using a JEOL-2100 and a Philips CM20 microscope both operating at 200 kV. Specimens for study in the JEOL-2100 microscope were prepared using a precision ion polishing system (PIPS). Specimens for study in the Philips CM20 microscope were prepared by twin jet electropolishing with 30 % of nitric acid in methanol at −20 °C at an operating voltage of 12 V. Qualitative energy dispersive X-ray (EDX) analysis was performed using an Oxford link model MK6 ultra-thin window EDX detector with a focused electron beam attached to the Philips CM20 microscope. The nominal beam diameter was 2 nm. Observations were made in both the bright and the dark field imaging modes, and selected area electron diffraction (SAED) patterns were recorded from areas of interest using an aperture of 1.1 μm nominal diameter. Misorientations between the grains were studied by analyzing the diffraction patterns using the microbeam diffraction technique. The microbeam patterns were obtained using a nominal probe diameter of 15 nm. The samples were tilted to different angles to reveal the presence or the absence of dislocations within grains. The dislocation density ρ was estimated by means of the line intercept method [12] as

$$\rho = 2N/Lt \tag{1}$$

where N is the number of intersections with dislocations, L is the total length of random lines, and t is the foil thickness, which was taken as 100 nm [12].

Tensile specimens with gauge length 7.5 mm, gauge width 1.5 mm and gauge thickness ~1.2 mm were machined from the ECAP-processed samples. The tensile axis of the specimens was parallel to the pressing direction. At the final stage of preparation, these tensile specimens were mechanically polished using silica colloidal solution. A few scratches were deliberately retained on the surface to be used as markers in subsequent experiments. Tensile tests were carried out using a 30 kN INSTRON universal testing machine. Tensile specimens of the ECAP processed material were deformed to failure with constant cross-head speeds corresponding to initial strain rates of 10^{-4}, 10^{-3}, 10^{-2}, and 10^{-1} s^{-1} at constant test temperatures of 20, 100, 150, 200, 250, 300, and 350 °C. Tensile tests at a strain rate of 1.1×10^{-5} s^{-1} were additionally performed at room temperature. Prior to the start of a tensile test, the specimen was kept for 30 min at the pre-set test temperature. The test temperature was measured by a thermocouple clamped to the upper shoulder of the tensile specimen with an accuracy of ±2 °C. Upon completion of the tensile test to failure, the furnace was immediately switched off and opened, and the sample was removed and quenched in water for rapid cooling. Analysis of the deformation relief of the tested samples was performed using a LEO-1530 scanning electron microscope (SEM) operated at 20 kV.

To study the anisotropy of deformation behavior at room temperature and estimate the strain rate sensitivity over a wide strain rate range, compression tests were also performed. Cubes 8 mm × 8 mm × 8 mm in size were machined for the compression tests. One of the side faces in each specimen was polished to a mirror-like surface using silica colloidal solution at the final stage. As with tensile specimens, a few scratches were deliberately retained on the surface. Compression tests were performed at room temperature at strain rates of 10^{-5}, 10^{-4}, 10^{-3}, and 10^{-2} s^{-1}. The compression axis was normal to a face of a cube-shaped specimen.

To estimate the strain rate sensitivity index, m, strain rate jump tests were conducted from the base strain rate of 10^{-3} s^{-1}. The strain between the strain rate jumps (~0.03) was sufficient for possible transient effects associated with the inertia of the testing machine to die off. The m-values were calculated using the following standard equation [13]

$$m = \frac{\partial \ln(\sigma)}{\partial \ln(\dot{\varepsilon})} \equiv \frac{\ln(\sigma_2/\sigma_1)}{\ln(\dot{\varepsilon}_2/\dot{\varepsilon}_1)} \tag{2}$$

where σ_2 and σ_1 are the values of the flow stress corresponding to the strain rates of $\dot{\varepsilon}_2$ and $\dot{\varepsilon}_1$, respectively. Back-extrapolation of the stress–strain curves to the strain at which a strain rate jump was made [13] was used to determine σ_2 and the corresponding instantaneous strain rate sensitivity. The activation volume V was estimated from the strain rate sensitivity index on the basis of the relation [13]

$$V = MkT(\mathrm{d}\ln\dot{\varepsilon}/\mathrm{d}\sigma) = MkT/(m\sigma) \tag{3}$$

where M is the Taylor factor (equal to 3.06 for Al with random texture), k is the Boltzmann constant, T is the absolute temperature, and σ is the flow stress.

3. Results

3.1. Mechanical behavior of the UFG Al–Mg–Si alloy in a wide temperature–strain rate range

Figure 1a illustrates a strong strain rate effect on the true stress–strain curves obtained from tensile tests at room temperature. The value of the uniform elongation increases from $\varepsilon_u = 2.1$ % at strain rate of $1.1 \cdot 10^{-5}$ s^{-1} to $\varepsilon_u = 20$ % at strain rate of 10^{-2} s^{-1}. The elongation to failure shows a similar behavior, increasing from $\delta = 8.2$ % to $\delta = 27.2$ %. Compression tests at room temperature did not reveal any tension–compression asymmetry in the UFG Al–Mg–Si alloy at low strain rates. Strain rate jump tests in the tensile mode at the lowest strain rate revealed increased strain rate sensitivity, $m \approx 0.03$. Strain rate jump tests in the compression mode at the same strain rate provided a similar m-value. However, the m-value shows a tendency to decrease with increasing base strain rate to $m \approx 0.013$ at the base strain rate of 10^{-2} s^{-1} (Fig. 1b). A detailed analysis of the stress–strain curves in tension and compression at room temperature was performed in [14, 15].

Figure 2a shows the true stress–true strain curves for elevated temperatures at the strain rate of 10^{-3} s^{-1}. The effect

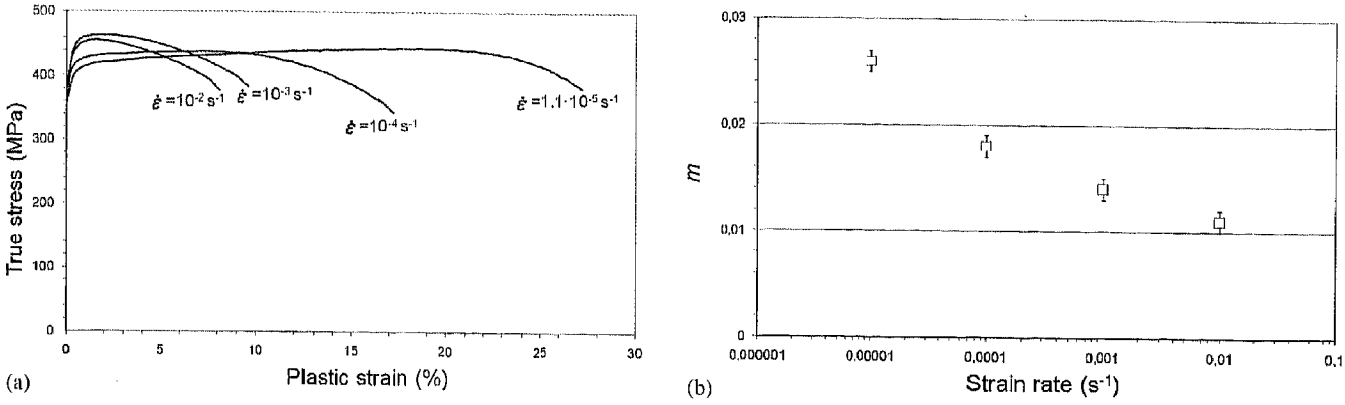

Fig. 1. (a) True stress–strain curves for the UFG Al–Mg–Si alloy tested at room temperature at different strain rates; (b) strain rate sensitivity index m vs. base strain rate.

of the strain rate on the deformation behavior at 200 °C is demonstrated in Fig. 2b. It is seen that the flow stress increases with increasing strain rate and decreasing test temperature. The typical stages of strain hardening leading up to quasi steady state deformation followed by necking can also be identified. (The post-necking parts of the curves in Fig. 2a and b are marked by thin lines). Detailed analysis of the deformation behavior of the UFG Al6082 alloy at elevated temperatures was performed in [16].

The m-values obtained for a fixed temperature did not vary with strain (or stress) within the scatter, but increased with temperature, ranging from 0.13 at 100 °C to 0.23 at 250 °C. The maximum scatter of m-values for a test conducted at a given temperature was ±0.02. The average m-values for different test temperatures are presented in Table 1.

Table 1. Data on strain rate sensitivity index, flow stress, and activation volume of the UFG Al–Mg–Si alloy during plastic deformation at the base strain rate of 10^{-3} s^{-1}.

T (°C)	100	150	200	250	300	350
m	0.13	0.17	0.16	0.20	0.17	0.21
σ (MPa)	305	189	100	61	38	26
V (b^3)	18	27	63	92	180	236

3.2. Microstructure of the ECAP-processed Al–Mg–Si alloy and its evolution during tensile tests

TEM studies of the material after ECAP processing and natural aging revealed a complex microstructure consisting of grains and subgrains with a size of 0.2–0.4 μm. Some high angle grain boundaries and low angle grain boundaries are marked by arrows in Fig. 3a and b, respectively. Such microstructure is typical of metals and alloys processed by ECAP [1, 2, 17]. Very fine recrystallized dislocation-free grains having a size of 0.09 μm are also observed in the microstructure (Fig. 3c). However, their fraction is very low. The alloy contains elongated second phase particles with an average length of 0.3 μm and width of 0.1 μm. These particles were identified as $Al_{12}Mn_3Si$ by EDX analysis. Tiny dispersoids, with an average size of 20 ± 3 nm, present in the microstructure, were identified as Mg_2Si. Both particles and dispersoids, were uniformly distributed within the matrix. No significant effect of deformation at room temperature on the microstructure was found. The dislocation density is seen to be high in most grains. Small recrystallized, dislocation-free nuclei similar to those for the specimen prior to tensile deformation were observed.

Annealing at 100–150 °C for 30 min resulted in recovery of the microstructure, the dislocation density within grains being significantly decreased. No grain growth was observed. Pre-annealing at 200 °C for 30 min resulted in grain growth. The grain size increased to 0.2–1.4 μm from the

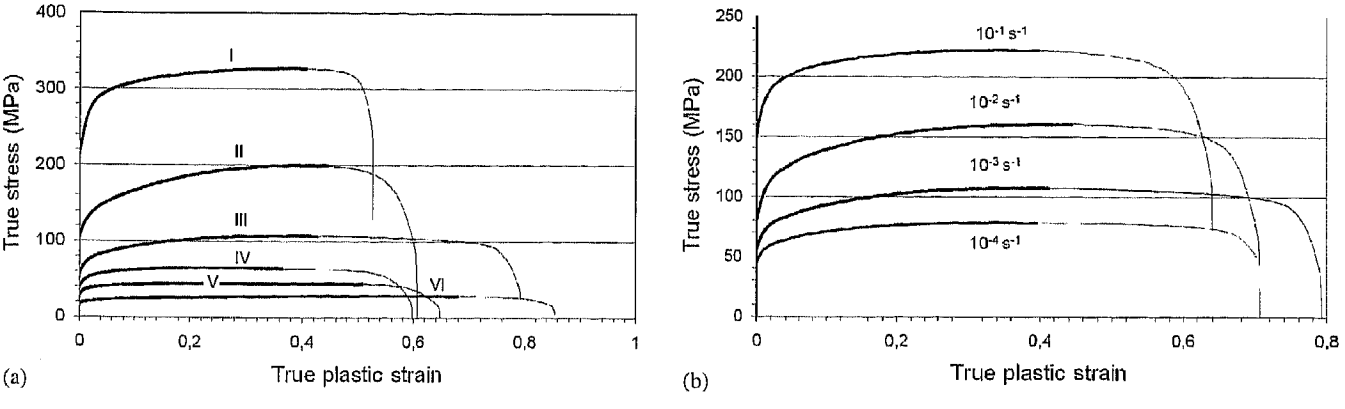

Fig. 2. True stress–strain curves limited to plastic region: (a) at a fixed strain rate of 10^{-3} s^{-1} (I – 100 °C, II – 150 °C, III – 200 °C, IV – 250 °C, V – 300 °C, VI – 350 °C); (b) at 200 °C for all strain rates.

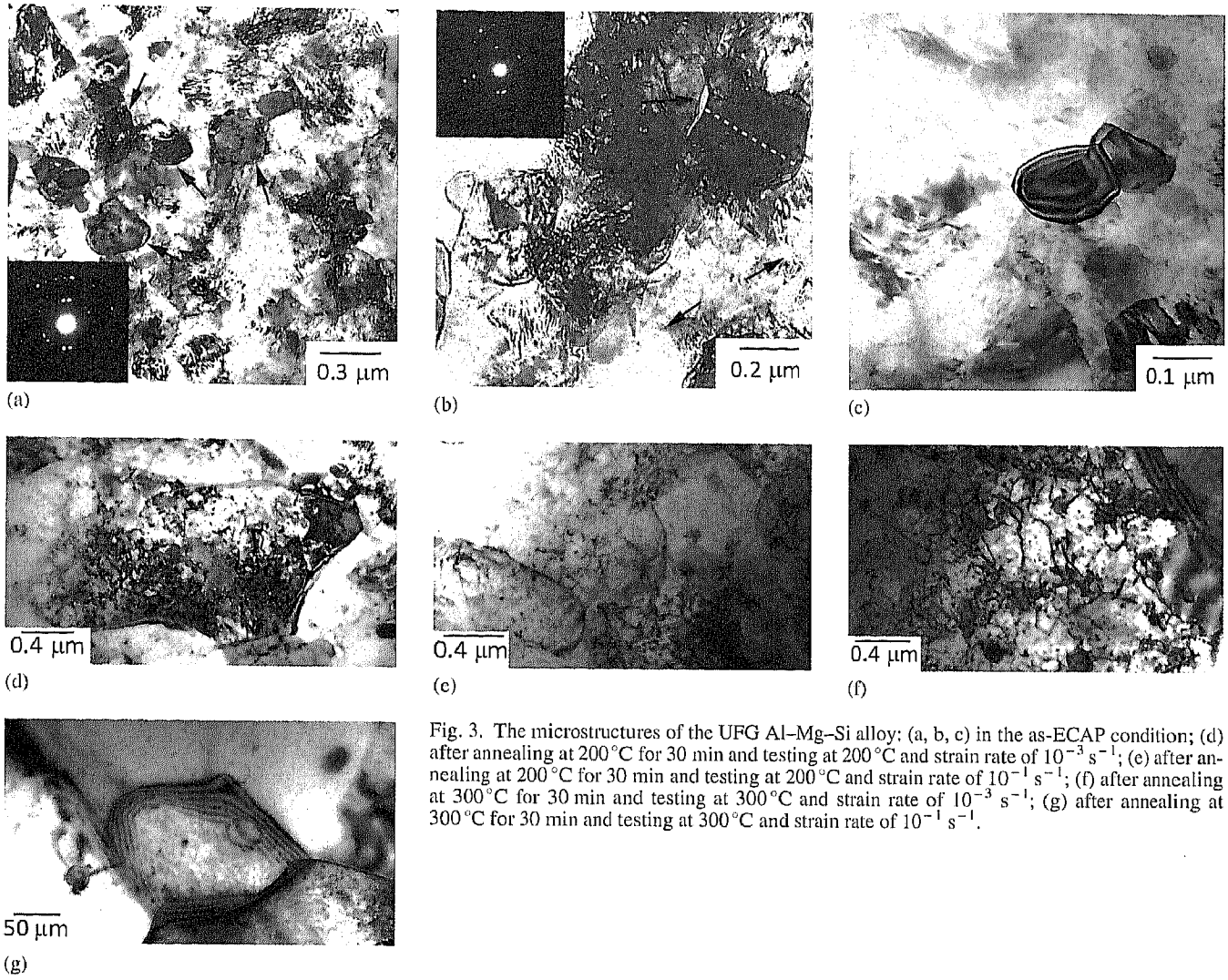

Fig. 3. The microstructures of the UFG Al–Mg–Si alloy: (a, b, c) in the as-ECAP condition; (d) after annealing at 200 °C for 30 min and testing at 200 °C and strain rate of 10^{-3} s^{-1}; (e) after annealing at 200 °C for 30 min and testing at 200 °C and strain rate of 10^{-1} s^{-1}; (f) after annealing at 300 °C for 30 min and testing at 300 °C and strain rate of 10^{-3} s^{-1}; (g) after annealing at 300 °C for 30 min and testing at 300 °C and strain rate of 10^{-1} s^{-1}.

initial values of 0.2–0.4 μm. The equiaxed grains had a relatively low dislocation density ($\rho = 10^{13}$ m^{-2}). TEM study of the samples after tensile testing at 200 °C at a strain rate of 10^{-3} s^{-1} did not reveal any significant microstructural changes (Fig. 3d). The dislocation density was in the range of $3.9 \cdot 10^{13} - 8.5 \cdot 10^{13}$ m^{-2}. Higher dislocation density of $\rho = 2 \cdot 10^{14}$ m^{-2} was observed in the samples tested at the strain rate of 10^{-1} s^{-1} (Fig. 3e). Grain boundaries appeared to be pinned by second phase precipitates. Significant growth of second phase precipitates was observed. For instance, in the sample tested at strain rate of $10^{-3}s^{-1}$, the Mg_2Si particles grew to an average size of 100 nm.

Substantial grain coarsening to an average size of 2.6 μm was observed after pre-annealing at 300 °C for 30 min. Grain boundaries again appeared to be pinned by precipitates. TEM of the samples after tensile testing at the strain rate of 10^{-3} s^{-1} revealed a bi-modal microstructure similar to that observed in the SEM (see Section 3.3). Dislocation density within the coarse grains increased to $\rho = 1.9 \cdot 10^{14}$ m^{-2} (Fig. 3f). However, there were also ultra-fine grains that were free of interior dislocations. A similar microstructure was observed in the specimen tested at 300 °C at a strain rate of 10^{-1} s^{-1}. An increase of the strain rate to the highest value used (10^{-1} s^{-1}) resulted in an increased dislocation density in the coarse grains ($\rho = 4.1 \cdot 10^{14}$ m^{-2}). Ultra-fine grains free of dislocations were still present (Fig. 3g). There was a significant growth of second phase precipitates. For example, the average size of the Mg_2Si particles grew to 0.21 μm in the sample tested at 300 °C with the strain rate of 10^{-3} s^{-1}.

3.3. Analysis of the deformation relief of the UFG Al–Mg–Si alloy

SEM analysis of the tensile specimens showed a strong effect of strain rate on the deformation relief. Micro shear bands with a thickness of 200 nm to 4 μm were observed on the surface of the specimen tested at the lowest strain rate of $1.1 \cdot 10^{-5}$ s^{-1} (Fig. 4a). This is confirmed by kinks in the scratches on the specimen surface which were initially straight. The micro shear bands were homogeneously distributed over the entire gauge section and were inclined at 45° to the tensile axis. The tensile strain associated with a micro shear band can be estimated for each individual micro shear band by tracing the displacements in the polishing scratches across the band. The area fraction of micro shear bands was found to be 18.4% [18]. The total contribution of micro shear banding to the total uniform elongation of the sample tested at the lowest strain rate was estimated at 9.6% (of 20%) [18]. No micro shear bands were observed on the surface of the samples tested at the high strain rates of 10^{-3} s^{-1} and 10^{-2} s^{-1}.

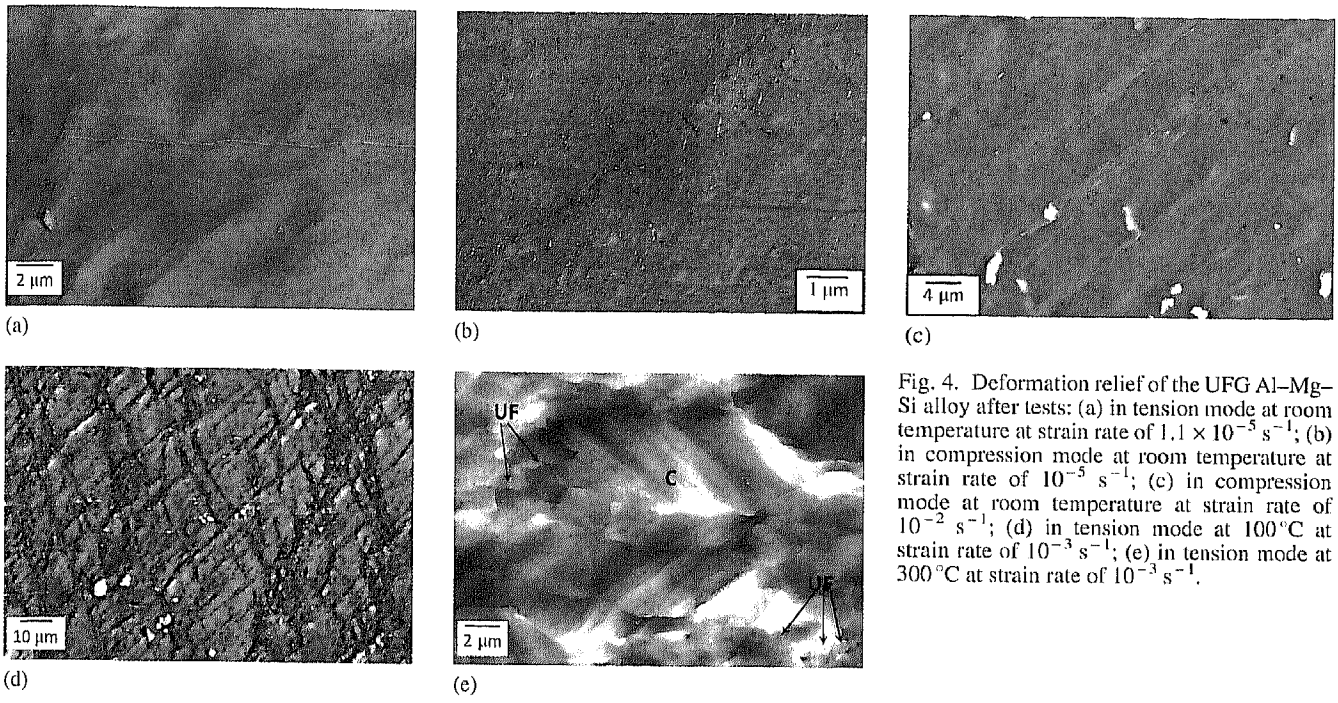

Fig. 4. Deformation relief of the UFG Al–Mg–Si alloy after tests: (a) in tension mode at room temperature at strain rate of 1.1×10^{-5} s^{-1}; (b) in compression mode at room temperature at strain rate of 10^{-5} s^{-1}; (c) in compression mode at room temperature at strain rate of 10^{-2} s^{-1}; (d) in tension mode at 100 °C at strain rate of 10^{-3} s^{-1}; (e) in tension mode at 300 °C at strain rate of 10^{-3} s^{-1}.

The deformation relief of the samples tested in the compression mode at the lowest strain rate was similar to that observed on the samples tested in tension. Individual grains can easily be detected within a micro shear band. However, they are not resolved in the areas outside of a micro shear band (Fig. 4b). In this case, though, the formation of shear bands was also observed in the samples tested at higher strain rates (10^{-2} s^{-1}). However, their morphology is completely different; they are similar to persistent slip band (PSB)-like shear bands observed earlier in ultra-fine-grained Cu subjected to fatigue loading [19–21]. Firstly, these PSB-like shear bands are thinner than the micro shear bands described above and, secondly, they are significantly longer than the micro shear bands (the longest ones observed being 500 μm in size) and are also more widely spaced (Fig. 4c). Individual grains could be detected neither within these PSB-like shear bands nor in the areas outside. Micro cracks up to 1 μm long and oriented at ~45° to the compression axis were also observed.

The deformation relief on the surface of the tensile samples tested at the elevated temperatures was also carefully examined. At low temperatures, in the range of 100–150°C, the deformation behavior has an inhomogeneous character at all strain rates. Extensive micro shear banding is observed throughout the gauge length (Fig. 4d). The thickness of the micro shear bands was 1–4 μm and the maximum length of shear bands observed in a shear plane was 40 μm. The shear bands were inclined at 35–55° to the tensile axis. At higher test temperatures, the deformation relief was more homogeneous. An increase in tensile test temperature to 200 °C resulted in the formation of a bi-modal microstructure at all strain rates. Coarse grains, elongated in the tensile direction with a length of 10–15 μm and a width of 3–6 μm, were embedded in a "matrix" of equiaxed ultra-fine grains 0.2–1 μm in size. In Fig. 4e, a coarse grain is marked as C, and the areas of ultra-fine grains as marked as UF. Slip lines were observed within the coarse elongated grains (Fig. 4e). There was also evidence of cooperative grain boundary sliding, resulting in local shearing along grain boundaries. There was no strong effect of strain rate on the surface relief and microstructure.

4. General discussion

From the results presented above, it is clearly seen that the mechanisms operating during plastic deformation are influenced by the test parameters: temperature and strain rate. Some deformation mechanisms appear to be active for all temperature–strain rate conditions studied here. Thus, a simple analysis of the true stress–true strain curves shows the importance of the dislocation glide at all temperatures and strain rates (Fig. 1a, Fig. 2). Strain hardening (which is related to an increase in the dislocation density with increasing strain) was observed for all specimens tested at all temperatures and strain rates, although the amount of strain hardening depends on the values of these parameters (see Section 3.1.). It appears that other deformation mechanisms are active only at certain temperatures and strain rates. Some features of the plastic deformation behavior of the alloy studied are discussed below.

4.1. Plastic deformation of the UFG Al–Mg–Si alloy at room temperature

From the results presented above it is clearly seen that the homogeneity of plastic deformation at room temperature strongly depends on the strain rate. Extensive micro shear banding observed at the lowest strain rate of $1.1 \cdot 10^{-5}$ s^{-1} is suppressed at higher strain rates, $10^{-3} - 10^{-2}$ s^{-1}. We have previously suggested that this micro shear banding (or localization of plastic deformation at the micro scale) is due to grain boundary sliding [14, 18] which is, in turn, activated by grain boundary diffusion [15]. The increased volume fraction of grain boundaries in the UFG material studied should promote grain boundary diffusion processes.

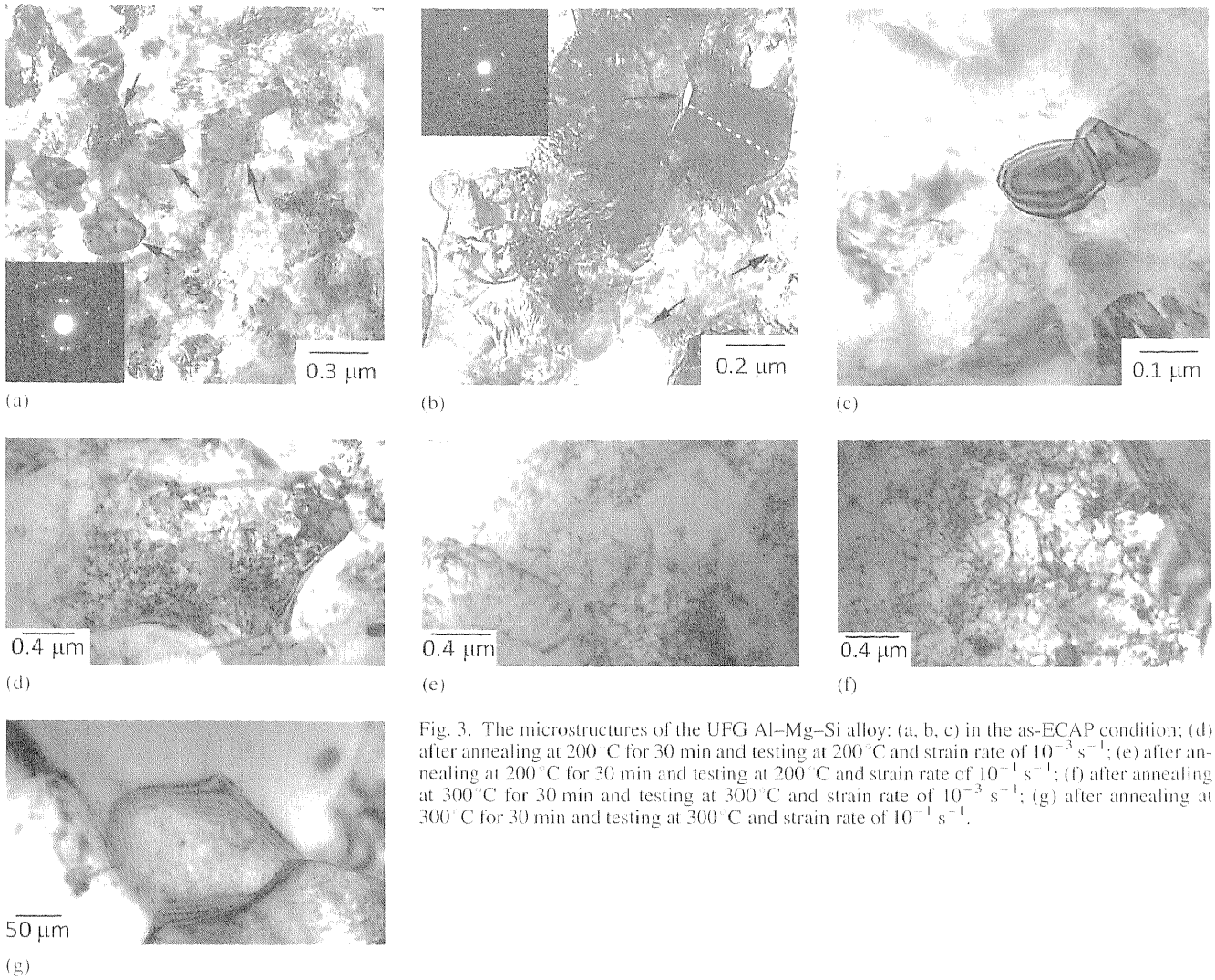

Fig. 3. The microstructures of the UFG Al–Mg–Si alloy: (a, b, c) in the as-ECAP condition; (d) after annealing at 200 °C for 30 min and testing at 200 °C and strain rate of 10^{-3} s^{-1}; (e) after annealing at 200 °C for 30 min and testing at 200 °C and strain rate of 10^{-1} s^{-1}; (f) after annealing at 300 °C for 30 min and testing at 300 °C and strain rate of 10^{-3} s^{-1}; (g) after annealing at 300 °C for 30 min and testing at 300 °C and strain rate of 10^{-1} s^{-1}.

initial values of 0.2–0.4 μm. The equiaxed grains had a relatively low dislocation density ($\rho = 10^{13}$ m^{-2}). TEM study of the samples after tensile testing at 200 °C at a strain rate of 10^{-3} s^{-1} did not reveal any significant microstructural changes (Fig. 3d). The dislocation density was in the range of $3.9 \cdot 10^{13} - 8.5 \cdot 10^{13}$ m^{-2}. Higher dislocation density of $\rho = 2 \cdot 10^{14}$ m^{-2} was observed in the samples tested at the strain rate of 10^{-1} s^{-1} (Fig. 3e). Grain boundaries appeared to be pinned by second phase precipitates. Significant growth of second phase precipitates was observed. For instance, in the sample tested at strain rate of $10^{-3}s^{-1}$, the Mg_2Si particles grew to an average size of 100 nm.

Substantial grain coarsening to an average size of 2.6 μm was observed after pre-annealing at 300 °C for 30 min. Grain boundaries again appeared to be pinned by precipitates. TEM of the samples after tensile testing at the strain rate of 10^{-3} s^{-1} revealed a bi-modal microstructure similar to that observed in the SEM (see Section 3.3). Dislocation density within the coarse grains increased to $\rho = 1.9 \cdot 10^{14}$ m^{-2} (Fig. 3f). However, there were also ultra-fine grains that were free of interior dislocations. A similar microstructure was observed in the specimen tested at 300 °C at a strain rate of 10^{-1} s^{-1}. An increase of the strain rate to the highest value used (10^{-1} s^{-1}) resulted in an increased dislocation density in the coarse grains ($\rho = 4.1 \cdot 10^{14}$ m^{-2}). Ultra-fine grains free of dislocations were still present (Fig. 3g). There was a significant growth of second phase precipitates. For example, the average size of the Mg_2Si particles grew to 0.21 μm in the sample tested at 300 °C with the strain rate of 10^{-3} s^{-1}.

3.3. Analysis of the deformation relief of the UFG Al–Mg–Si alloy

SEM analysis of the tensile specimens showed a strong effect of strain rate on the deformation relief. Micro shear bands with a thickness of 200 nm to 4 μm were observed on the surface of the specimen tested at the lowest strain rate of $1.1 \cdot 10^{-5}$ s^{-1} (Fig. 4a). This is confirmed by kinks in the scratches on the specimen surface which were initially straight. The micro shear bands were homogeneously distributed over the entire gauge section and were inclined at 45° to the tensile axis. The tensile strain associated with a micro shear band can be estimated for each individual micro shear band by tracing the displacements in the polishing scratches across the band. The area fraction of micro shear bands was found to be 18.4% [18]. The total contribution of micro shear banding to the total uniform elongation of the sample tested at the lowest strain rate was estimated at 9.6% (of 20%) [18]. No micro shear bands were observed on the surface of the samples tested at the high strain rates of 10^{-3} s^{-1} and 10^{-2} s^{-1}.

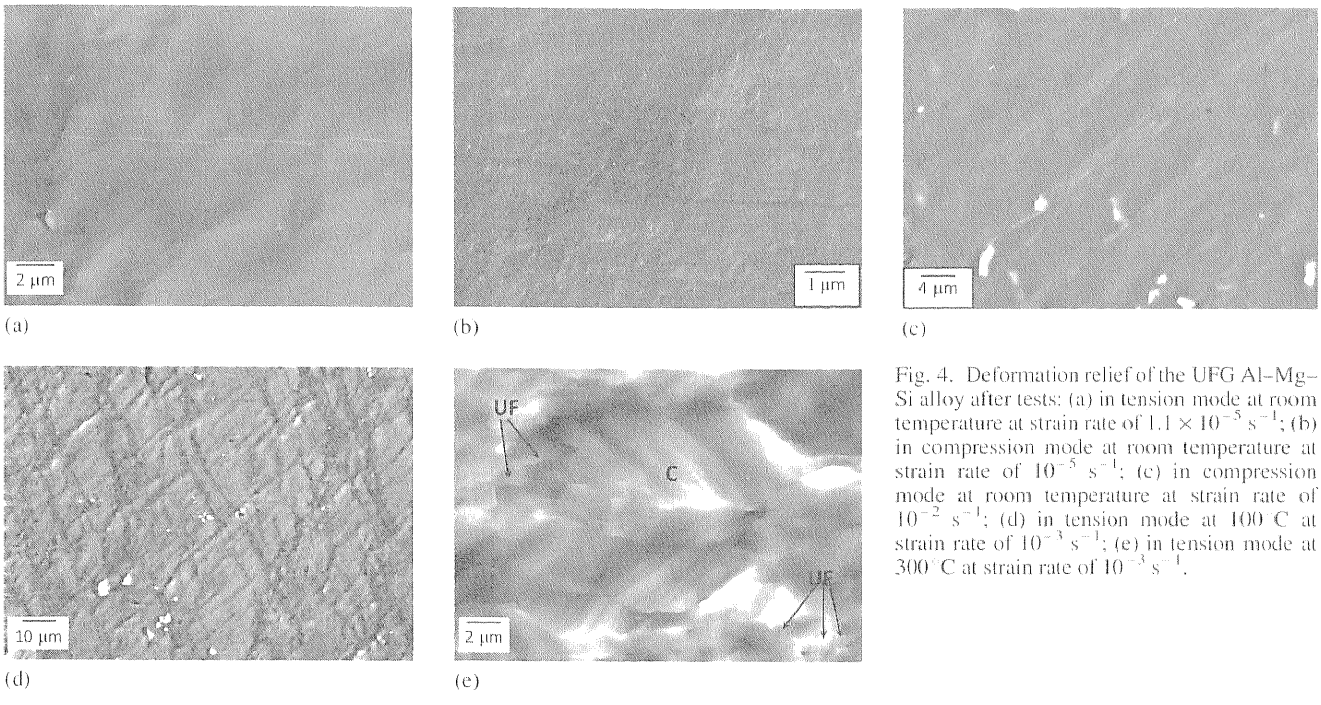

Fig. 4. Deformation relief of the UFG Al–Mg–Si alloy after tests: (a) in tension mode at room temperature at strain rate of 1.1×10^{-5} s^{-1}; (b) in compression mode at room temperature at strain rate of 10^{-5} s^{-1}; (c) in compression mode at room temperature at strain rate of 10^{-2} s^{-1}; (d) in tension mode at 100 °C at strain rate of 10^{-3} s^{-1}; (e) in tension mode at 300 °C at strain rate of 10^{-3} s^{-1}.

The deformation relief of the samples tested in the compression mode at the lowest strain rate was similar to that observed on the samples tested in tension. Individual grains can easily be detected within a micro shear band. However, they are not resolved in the areas outside of a micro shear band (Fig. 4b). In this case, though, the formation of shear bands was also observed in the samples tested at higher strain rates (10^{-2} s^{-1}). However, their morphology is completely different; they are similar to persistent slip band (PSB)-like shear bands observed earlier in ultra-fine-grained Cu subjected to fatigue loading [19–21]. Firstly, these PSB-like shear bands are thinner than the micro shear bands described above and, secondly, they are significantly longer than the micro shear bands (the longest ones observed being 500 μm in size) and are also more widely spaced (Fig. 4c). Individual grains could be detected neither within these PSB-like shear bands nor in the areas outside. Micro cracks up to 1 μm long and oriented at ~45° to the compression axis were also observed.

The deformation relief on the surface of the tensile samples tested at the elevated temperatures was also carefully examined. At low temperatures, in the range of 100–150 °C, the deformation behavior has an inhomogeneous character at all strain rates. Extensive micro shear banding is observed throughout the gauge length (Fig. 4d). The thickness of the micro shear bands was 1–4 μm and the maximum length of shear bands observed in a shear plane was 40 μm. The shear bands were inclined at 35–55° to the tensile axis. At higher test temperatures, the deformation relief was more homogeneous. An increase in tensile test temperature to 200 °C resulted in the formation of a bi-modal microstructure at all strain rates. Coarse grains, elongated in the tensile direction with a length of 10–15 μm and a width of 3–6 μm, were embedded in a "matrix" of equiaxed ultra-fine grains 0.2–1 μm in size. In Fig. 4e, a coarse grain is marked as C, and the areas of ultra-fine grains as marked as UF. Slip lines were observed within the coarse elongated grains (Fig. 4e). There was also evidence of cooperative grain boundary sliding, resulting in local shearing along grain boundaries. There was no strong effect of strain rate on the surface relief and microstructure.

4. General discussion

From the results presented above, it is clearly seen that the mechanisms operating during plastic deformation are influenced by the test parameters: temperature and strain rate. Some deformation mechanisms appear to be active for all temperature–strain rate conditions studied here. Thus, a simple analysis of the true stress–true strain curves shows the importance of the dislocation glide at all temperatures and strain rates (Fig. 1a, Fig. 2). Strain hardening (which is related to an increase in the dislocation density with increasing strain) was observed for all specimens tested at all temperatures and strain rates, although the amount of strain hardening depends on the values of these parameters (see Section 3.1.). It appears that other deformation mechanisms are active only at certain temperatures and strain rates. Some features of the plastic deformation behavior of the alloy studied are discussed below.

4.1. Plastic deformation of the UFG Al–Mg–Si alloy at room temperature

From the results presented above it is clearly seen that the homogeneity of plastic deformation at room temperature strongly depends on the strain rate. Extensive micro shear banding observed at the lowest strain rate of $1.1 \cdot 10^{-5}$ s^{-1} is suppressed at higher strain rates, $10^{-3} - 10^{-2}$ s^{-1}. We have previously suggested that this micro shear banding (or localization of plastic deformation at the micro scale) is due to grain boundary sliding [14, 18] which is, in turn, activated by grain boundary diffusion [15]. The increased volume fraction of grain boundaries in the UFG material studied should promote grain boundary diffusion processes.

The importance of diffusion at a given temperature should increase with decreasing strain rate. Indeed, the strain rate sensitivity index m was found to increase with decreasing strain rate (Fig. 1b). Although the direct contribution of grain boundary diffusion to plastic strain is very low (or even negligible), it can be sufficient for the activation of some grain boundary sliding if the material is tested at very low strain rates (such as 10^{-5} s^{-1}) [18].

It is clear that tensile ductility at room temperature is controlled by the localization of plastic deformation at the macro scale. Although, in general, shear banding is known to reduce ductility of the UFG and nanostructured materials, it can be exploited to improve their tensile ductility if it is activated at the micro-scale [18]. The key to ductility is a fine scale distribution of micro shear bands that acts against larger scale localization in macro shear bands. Manipulation of the mechanisms of plastic deformation seems to be the only way to achieve this. As demonstrated here, this can be done by tuning the test parameters: strain rate and temperature.

4.2. Plastic deformation of the UFG Al–Mg–Si alloy at elevated temperatures

Due to the complexity of the microstructure in the ECAP-processed material, it is difficult to identify any difference between the as-ECAP specimens and the specimens subsequently deformed in tension or compression at room temperature. However, the effect of the plastic deformation on the microstructure is very clearly seen in the as-ECAP specimens tested at elevated temperatures. This is due to the recovery of the as-ECAP microstructure or even grain growth (see Section 3.2.) during pre-annealing before tensile testing.

An increase in the test temperature to 100–150 °C results in the activation of micro shear banding at all strain rates. This effect also supports the proposed mechanism for the formation of micro shear bands at room temperature (see Section 4.1.). Indeed, it appears that an increase in test temperature can allow grain boundary diffusion at higher strain rates promoting grain boundary sliding also at the higher strain rates. An interesting finding is the development of bi-modal microstructure during testing at elevated temperatures (200–300 °C) at all strain rates considered. Detailed TEM analysis of the microstructure revealed profuse dislocation activity in coarse grains, whereas no dislocations were observed in the very fine grains. Two explanations were proposed for this effect [16]:

1. The generated dislocations move across the ultra-fine grains and disappear at grain boundaries. The absence of fine precipitates within the ultra-fine grains, which could pin dislocations (Fig. 3g), supports this explanation.
2. Plastic deformation in the ultra-fine and nano grains at elevated temperatures is diffusion controlled.

Although the entirety of the experimental data gathered in [14–16, 18] and reviewed here suggests that dislocation glide is the main deformation mechanism within the coarse grains, dislocation forests are not widely observed in the microstructure of the UFG Al–Mg–Si alloy tested at elevated temperatures, irrespective of the strain rate applied. It can be assumed that the second phase precipitates are not able to act as barriers for dislocation glide as at these temperatures they can be overcome by climb [22]. This can also lead to a decrease in the dislocation density by their annihilation, for instance, through the mechanism proposed by Weertman [23].

The enhanced strain rate sensitivity at elevated temperatures may be associated with a larger contribution of the grain boundary mediated deformation mechanisms (grain boundary sliding and grain boundary diffusion) compared to the situation at room temperature as well as with climb controlled annihilation of lattice dislocations [24–26]. In reference [27], the strain rate sensitivity of an UFG Al6061 alloy processed by ECAP was studied over a wide temperature range. It should be noted that the m-values measured for the UFG Al6061 in [27] are comparable with the m-values obtained for our material at 200 °C and above. Thermally activated recovery processes at the grain boundaries were suggested to be the rate-controlling deformation mechanisms for the UFG Al6061 [27]. Analysis of the deformation mechanisms in an UFG Al6082 at elevated temperatures was performed in [16] in order to determine the predominant one. The grain boundary mediated mechanisms were ruled out since

(i) the maximum value of the strain rate sensitivity index m did not exceed 0.21 and
(ii) no signature of superplastic behavior was observed [16].

Overcoming of precipitates by thermal activation according to Seeger's model as the mechanism controlling dislocation glide was discarded, as well [16]. Estimation of the activation volume for the present UFG alloy Al6082 yields values between 18 b^3 and 236 b^3, the magnitude of the activation volume being inversely proportional to the flow stress (Tab. 1). On this basis, it was suggested [16] that the rate-controlling thermally activated process is likely to be associated with the overcoming of forest junctions by gliding dislocations [12].

5. Conclusions

An ultra-fine grained Al–Mg–Si alloy (Al6082) was produced by equal channel angular pressing. The deformation behavior of the material was studied over a wide range of temperatures and strain rates. It was demonstrated that activation of micro shear banding, especially their diffuse fine scale distribution, can be utilized to significantly increase room temperature ductility. Extensive micro shear banding in samples tested at 100–150 °C over a wide strain rate range was found. A bi-modal microstructure in the samples tested at higher temperatures was observed. It was demonstrated that dislocation glide is active only in coarse grains, whereas no evidence of dislocation activity within very fine grains was found. It was suggested that the results of the analysis of the activation volume for the thermally activated plastic deformation is consistent with the assumption that plastic deformation in the coarse-grain fraction of the bi-modal grain population is controlled by the overcoming of forest junctions by gliding dislocations.

The authors acknowledge financial support from the Australian Research Council through the ARC Centre of Excellence for Design in Light Metals and the Federation Fellowship awarded to PH. IS and MB would like to thank Deakin University for partial funding through the Central Research Grants Scheme.

References

[1] R.Z. Valiev, Y. Estrin, Z. Horita, T.G. Langdon, M.J. Zehetbauer, Y.T. Zhu: J. Mater. 58 (2006) 33–39.
[2] R.Z. Valiev, T.G. Langdon: Prog. Mater. Sci. 51 (2006) 881–981. DOI:10.1016/j.pmatsci.2006.02.003
[3] I.J. Polmear: Light Alloys – Metallurgy of the Light Metals, Arnold, London (1995).
[4] R. Islamgaliev, N. Yunusova, I. Sabirov, A. Sergueeva, R. Valiev: Mater. Sci. Eng. A 319–321 (2001) 877–881. DOI:10.1016/S0921-5093(01)01052-8
[5] E. Ma: J. Metal. 58(4) (2006) 49–58.
[6] Y.M. Wang, M. Chen, F. Zhou, E. Ma: Nature 419 (2002) 912–915. PMid:12410306; DOI:10.1038/nature01133
[7] Y.M. Wang, E. Ma: Acta Mater. 52 (2004) 1699–1709. DOI:10.1016/j.actamat.2003.12.022
[8] B.Q. Han, Z. Lee, D. Witkin, S. Nutt, E.J. Lavernia: Metall. Mater. Trans. A 36 (2005) 957–965. DOI:10.1007/s11661-005-0289-7
[9] Y.H. Zhao, X.Z. Liao, S. Cheng, E. Ma, Y.T. Zhu: Adv. Mater. 18 (2006) 2280–2283. DOI:10.1002/adma.200600310
[10] T. Shanmugasundaram, B.S. Murty, V. Subramanya Sarma: Scripta Mater. 54 (2006) 2013–2017. DOI:10.1016/j.scriptamat.2006.03.012
[11] E.V. Hart: Acta Metall. 15 (1967) 351–355. DOI:10.1016/0001-6160(67)90211-8
[12] P.B. Hirsch, R.B. Nicholson, A. Howie, D.W. Pashley, M.J. Whelan: Electron Microscopy of Thin Crystals, Butterworths, London (1965).
[13] D. Caillard, J.L. Martin: Thermally Activated Mechanisms in Crystal Plasticity, Pergamon Materials Series, Vol. 8, Elsevier. Oxford (2003). DOI:10.1016/S1470-1804(03)80029-9
[14] I. Sabirov, Y. Estrin, M.R. Barnett, I. Timokhina, P.D. Hodgson: Scripta Mater. 58 (2008) 163–166.
[15] I. Sabirov, M.R. Barnett, Y. Estrin, P.D. Hodgson: Scripta Mater. 61 (2009) 181–184. DOI:10.1016/j.scriptamat.2009.03.032
[16] B.P. Kashyap, P.D. Hodgson, Y. Estrin, I. Timokhina, M.R. Barnett, I. Sabirov: Metall. Mater. Trans. A 40 (2009) 3294–3303. DOI: 10.1007/s11661-009-0036-6.
[17] T. Hebesberger, H.P. Stuewe, A. Vorhauer, F. Wetscher, R. Pippan: Acta Mater. 53 (2005) 393–402. DOI:10.1016/j.actamat.2004.09.043
[18] I. Sabirov, Y. Estrin, M.R. Barnett, I. Timokhina, P.D. Hodgson: Acta Mater. 56 (2008) 2223–2230. DOI:10.1016/j.actamat.2008.01.020
[19] S.R. Agnew, J.R. Weertman: Mater. Sci. Eng. A 244 (1998) 145–153. DOI:10.1016/S0921-5093(97)00689-8
[20] S.D. Wu, Z.G. Wang, C.B. Jiang, G.Y. Li, I.V. Alexandrov, R.Z. Valiev: Mater. Sci. Eng. A 387–389 (2004) 560–564. DOI:10.1016/j.msea.2003.12.087
[21] S.D. Wu, Z.G. Wang, C.B. Jiang, G.Y. Li, I.V. Alexandrov, R.Z. Valiev: Scripta Mater. 48 (2003) 1605–1609. DOI:10.1016/S1359-6462(03)00141-6
[22] R. Kaibyshev, O. Sitdikov, I. Mazurina, D.R. Lesuer: Mater. Sci. Eng. A 334 (2002) 104–113. DOI:10.1016/S0921-5093(01)01777-4
[23] J.R. Weertman: J. Appl. Phys. 28 (1957) 362–366. DOI:10.1063/1.1722747
[24] J. May, H.W. Hoeppel, M. Goeken: Scripta Mater. 53 (2005) 189–194. DOI:10.1016/j.scriptamat.2005.03.043
[25] Y.J. Li, X.H. Zeng, W. Blum: Acta Mater. 52 (2004) 5009–5018. DOI:10.1016/j.actamat.2004.07.003
[26] W. Blum, X.H. Zeng: Acta Mater. 57 (2009) 1966–1974. DOI:10.1016/j.actamat.2008.12.041
[27] A. Vevecka-Priftaj, A. Boehner, J. May, H.W. Hoeppel, M. Goeken: Mater. Sci. Forum. 584–586 (2008) 741–747. DOI:10.4028/www.scientific.net/MSF.584-586.741

(Received May 26, 2009; accepted October 15, 2009)

Bibliography

DOI 10.3139/146.110239
Int. J. Mat. Res. (formerly Z. Metallkd.)
100 (2009) 12; page 1679–1685

ISSN 1862-5282

Correspondence address

Dr. Ilchat Sabirov
IMDEA Materials
Calle Profesor Aranguren, E.T.S. de Ingenieros de Caminos
Madrid, 28040, Spain
Tel.: +34 9 1549 3422
Fax: +34 9 1550 3047
E-mail: ilchat.sabirov@imdea.org

You will find the article and additional material by entering the document number **MK110239** on our website at *www.ijmr.de*